THE JOURNAL OF PHYSICAL CHEMISTRY C

Article

pubs.acs.org/JPCC

Role of WO_3 in the Hg Oxidation across the V_2O_5–WO_3–TiO_2 SCR Catalyst: A DFT Study

Ana Suarez Negreira and Jennifer Wilcox*

Department of Chemical Engineering and Department of Energy Resources Engineering, Stanford University, Stanford, California 94305, United States

ABSTRACT: Selective catalytic reduction (SCR) units can be exploited to reduce Hg emissions from coal-based power plants; hereby, Hg^0 is oxidized into Hg^{2+}, which has a higher solubility than the former and can therefore be scrubbed before leaving the stacks. With the purpose of examining the effect of the surface composition and surface coverage on the reactivity of a commercial SCR catalyst (V_2O_5–WO_3–TiO_2) toward Hg oxidation, two models were used to represent TiO_2-supported systems with low and high loading of the two active phases (i.e., V_2O_5 and WO_3). The reactivities of these systems were compared through the analysis of the adsorption energies of Hg, Cl•, HgCl, and HCl, which are likely involved in the Hg oxidation mechanism. These adsorption energies were complemented by results from both the Bader charge and projected density of states (PDOS) analyses, thus providing an increased understanding of the effects of surface coverage and composition on the electronic structure of these materials. An enhanced reactivity of the SCR catalyst is observed with increasing loadings of both V_2O_5 and WO_3 phases. Binary systems (i.e., V_2O_5–TiO_2 or WO_3–TiO_2) were compared against ternary systems (V_2O_5–WO_3–TiO_2 with different V_2O_5/WO_3 ratios) and indicate a higher reactivity of the latter.

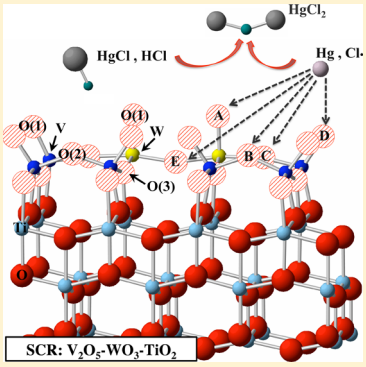

INTRODUCTION

The annual estimation of Hg emission from natural and coal-fired power plants in the United States corresponds to 48 tons, about one-third of the total amount of mercury released by anthropogenic sources of this country.[1] As the environmental and health problems associated with the mercury emissions from stationary sources become an obvious problem, the U.S. Environment Protection Agency set in 2011 a series of emission standards to limit these emissions. These standards state that the U.S. natural gas and coal-fired power plants are forced to install air pollution control devices to prevent 91% of the Hg present in flue gas from being released.[2]

The insolubility and inertness of Hg^0 make its capture difficult. Promoting its oxidation along the path of the flue gas from the boiler to the stack is the best removal strategy using current emission control technologies. Mercury oxidation has been observed across the selective catalytic reduction (SCR) unit with a primary purpose of controlling NO_x emissions by reducing them to N_2 and water vapor using ammonia (NH_3). Employing an already existing air pollution control device such as the SCR unit to tackle the Hg problem is an attractive approach due to the lower economic invesment and the environmental and heath benefits of reducing Hg emissions.

Commercial SCR catalysts employ the anatase phase of TiO_2 as a support material for the active phases which consists of vanadium and tungsten oxides.[3,4] The vanadia phase V_2O_5 not only catalyzes NO_x reduction[5] and Hg^0 oxidation[6] but also the undesired SO_2 to SO_3 oxidation reaction.[7] It has been proven experimentally that higher catalytic activities are reached with increasing V_2O_5 loadings in the SCR catalyst;[3,8] however, the content of V_2O_5 is limited to less than 2 wt% to avoid the production of SO_3 and because higher loadings of V_2O_5 decreases the temperature at which the TiO_2 anatase-to-rutile phase transformation occurs.[9] This phase transformation leads to a decrease in the surface area and the catalyst activity. The addition of tungsten oxide, WO_3, can stabilize the anatase phase of TiO_2, thereby preserving this phase surface characteristics.[3,10] Furthermore, it has been shown that WO_3 can act as a chemical promoter since it reduces ammonia (NH_3) and sulfur dioxide (SO_2) oxidation and increases the number of Bronsted acid sites, which are critical for the NO_x reduction.[3,11,12]

The commercial composition of the SCR is <2 wt% of vanadia oxide, 10 wt % of tungsten oxide supported on anatase, TiO_2. However, this is the composition for an optimal performance of this catalyst toward NO_x reduction, and little is known about the optimal composition for Hg oxidation (i.e., Hg^0 oxidation). Therefore, it is important to understand how this reaction is affected by the changes in the surface composition and surface coverage. Understanding these effects can be used to select the vanadia and tungsten loadings that maximize Hg oxidation as a cobenefit of the SCR unit.

From a theoretical point of view, several studies have been carried out attempting to understand the effect of some of the components of the SCR catalyst on its reactivity. The role of the active phase on the SCR reactivity has been studied using models with different levels of complexity, from unsupported V_2O_5 systems[13−18] to TiO_2-supported monolayer V_2O_5 systems[19−21] to TiO_2-supported submonolayer V_2O_5 sys-

Received: August 4, 2013
Revised: October 25, 2013
Published: October 28, 2013

dx.doi.org/10.1021/jp407794g | J. Phys. Chem. C 2013, 117, 24397−24406

tems.[21−25] However, most of these studies were carried out to understand the reactivity of these systems for NO_x reduction, so knowlegde regarding the optimal vanadia loading for Hg oxidation is still lacking.

Furthermore, previous theoretical studies do not include the effect of tungsten trioxide (WO_3) on the catalytic activity, although it is present at 10 wt% in commercial SCR catalysts. The interaction between surface vanadia and tungsten species has been modeled using cluster approaches[11,26] but neglect to include the strong interaction between the two active phases and the support.[3] This ternary system follows a structure similar to that of the binary system (V_2O_5−TiO_2).[3,11] Higher NO_x conversions and higher selectivity to N_2 were obtained at lower temperatures in ternary systems compared to the binary systems with the same vanadia loading, indicating that WO_3 increases the activity of V_2O_5−TiO_2 catalysts.[3] Since one step during the NO_x reduction is the adsorption of NH_3, the latter may compete with Hg^0 for the actives sites on the SCR catalyst.[27] It is one of the aims of this work to investigate surface alterations upon addition of WO_3 and to quantify its effects on Hg oxidation.

Besides studying the structural and electronic changes that affect the stability and reactivity of this catalyst, another goal of the current work is to determine the optimal loading for both active phases, V_2O_5 and WO_3. This is done by modeling binary and ternary SCR catalyst within the submonolayer and monolayer regimes. The low vanadia loading (<2 wt%) systems is modeled as isolated vanadium oxide species with the vanadium atoms having 4-fold coordination structure suggested by experimental studies.[28−32] The effect of adding tungsten at this low loading is studied by replacing one of the vanadium atoms in the dimer by one tungsten atom, as was done by Broclawik et al.[26]

Larger loadings were modeled with supported monolayer systems where the surface of the TiO_2 support is completely covered by the active phases. Current literature suggests that tungsten avoids the sintering of the vanadia phase, by keeping the vanadia species isolated. With the purpose of modeling this effect, we replaced some of the atoms in the WO_3 monolayer model by vanadium. Five supported monolayer systems have been chosen to study the effect of tungsten: pure supported V_2O_5 monolayer on TiO_2(001) surface, three mixed V_2O_5−WO_3 monolayer on TiO_2(001) surfaces (with 25%, 50%, and 75% of V_2O_5), and a pure WO_3 monolayer on the TiO_2(001) surface.

The presence of chlorine species (HCl, Cl_2, and Cl radicals ($Cl^\bullet$ formed at high temperatures) in the flue gas plays an essential role in the mercury oxidation.[33−36] Senior and Linjewile[34] suggest that adsorbed Hg interacts with gas-phase HCl by a Eley−Rideal mechanism, while Niksa and Fujiwara[33] suggest a Langmuir−Hinshelwood mechanism in which Hg adsorbs and then reacts with HCl that has previously been adsorbed onto the V_2O_5 surface. There is a clear disagreement regarding the specific interactions of Hg, Cl species and the catalyst surface. For this reason, in this paper we seek to explain and reconcile some of the uncertainties related to Hg oxidation by analyzing the adsorption energies of Hg, $Cl^\bullet$, HgCl, and HCl, which are likely involved in this reaction. These adsorption energies were complemented by results from both the Bader charge and projected density of states (PDOS) analyses, thus providing an increased understanding of the effects of surface coverage and composition on the electronic structure of these materials. The results of this study may be used as a guide to optimize the SCR catalyst formulation to improve the Hg oxidation capacity.

COMPUTATIONAL METHODOLOGY

Density Functional Theory. Structural optimizations were peformed using plane-wave DFT calculations using the Vienna *ab initio* simulation package (VASP).[37] The Perdew−Burke−Enzerhoff generalized-gradient approximation (PBE, GGA) was used for the exchange-correlation functional.[38] For the TiO_2, V_2O_5, and WO_3 bulk calculations, a projector augmented wave (PAW)[39] pseudopotential was used with an optimized energy cutoff of 500 eV. The number of k-points for the Brillion zone integration was chosen according to a Monkhorst−Pack[40] grid of 6 × 6 × 6 with a convergence criterion of 10^{-4} eV. The purpose of these bulk calculations was to obtain a reference state for the stability of the vanadia and/or tungsten oxide anatase supported systems.

A three-layer-TiO_2 (001) asymmetric surface was used as a support with a 4 × 2 (15.18 × 7.59 Å^2) unit cell and the inclusion of a dipole correction. The slabs were separated by a vacuum space of 15 Å^2 to prevent interaction between periodic images and to cancel any dipole moment thereby created. The number of k-points used was 2 × 4 × 1. The position of all atoms were allowed to relax with the exception of the bottom layer kept fixed in their bulk positions throughout the calculations. The optimization of the slab was carried out in our previous work where it was shown that a reasonable representation of the support could be obtained with just three atomic layers.[41] The vanadia and tungsten oxide species were placed on the top part of the slab to model the supported systems.

Gas-phase species (Hg, HCl, $Cl^\bullet$, and HgCl) were calculated as isolated molecules in a 20 × 20 × 20 Å^3 periodic box. The bond lengths of HCl and HgCl molecules were found to be 1.28 and 2.45 Å, respectively, which are in excellent agreement with previously reported bond distances: 1.27 Å (experimental bond distance for HCl)[42] and 2.44 Å (DFT bond distance for HgCl).[43]

RESULTS

Modeling Low-Loading Active Phase SCR Catalysts: Submonolayer Regime. For the low-loading system, the vanadia dimer was modeled having 4-fold coordination, with two adjacent metal sites in a similar configuration to that found on the V_2O_5(100) surface. The optimization of this structure was done in our previous work.[41] In the vanadia dimer, there are three structurally inequivalent oxygen sites, also present in the V_2O_5(001) surface, namely the single coordinated oxygen, O(1), the bridging O(2) oxygen atom, and the anchoring O(2)* oxygen atom (between dimer and support). To study the effect of adding tungsten into this system, one of the metal sites of the vanadia dimer was replaced by a tungsten atom as done in an unsupported cluster system by Broclawik et al.[26] and Sun et al.[11] The isolated WO_3−TiO_2(001) dimer system was also modeled for comparison with the mixed system. This isolated system was modeled as a W_2O_6 dimer, based on experimental and DFT studies.[44−46] According to Zhai et al.,[46] the stability of this dimer structure is due to the fact that all the 12 valence electrons on the two W atoms are used to form W−O bonds, leading to a large HOMO−LUMO gap. A representation of the three supported isolated dimer systems is shown in Figure 1.

dx.doi.org/10.1021/jp407794g | J. Phys. Chem. C 2013, 117, 24397−24406

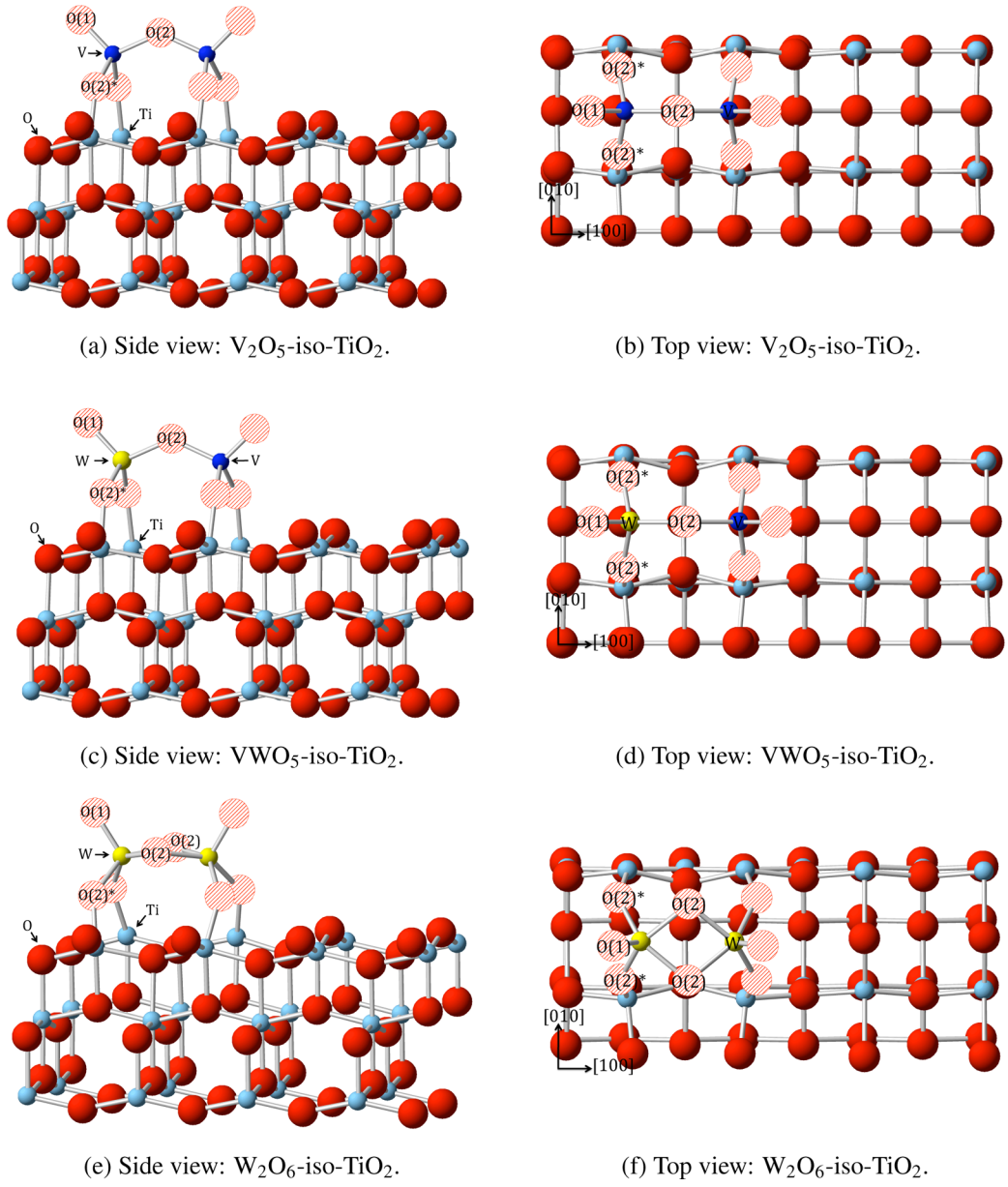

(a) Side view: V_2O_5-iso-TiO_2. (b) Top view: V_2O_5-iso-TiO_2.

(c) Side view: VWO_5-iso-TiO_2. (d) Top view: VWO_5-iso-TiO_2.

(e) Side view: W_2O_6-iso-TiO_2. (f) Top view: W_2O_6-iso-TiO_2.

Figure 1. Representation of binary and ternary TiO_2-supported low-loading active phase SCR catalysts.

The bond distances of the supported dimers were compared to previous DFT studies to benchmark the representation of these systems with low loading of the active phases. Although different computational methods were employed in these studies, there is a reasonable agreement among the bond distances summarized in Table 1. The bond distances for the mixed system VWO_5−iso-TiO_2 have not been reported previously so only the values obtained in this work are shown in Table 1.

Modeling High-Loading Active Phase SCR Catalysts: Monolayer Regime. For the monolayer regime, the V_2O_5−TiO_2(001) systems were modeled based on the work of Vittadini et al.,[20] who carried out a periodic DFT study of the energetics, structure, and electronic properties of vanadium oxide films grown on TiO_2(001) supports. They show that the epitaxial growth of vanadium oxide is favored in reducing conditions leading to pseudomorphic VO_2 films but that exposure to oxygen tends to restore V_2O_5 stoichiometry. This structure has been chosen to represent the titania-supported monolayer vanadia systems in the current work due to the high content of oxygen in the flue gas that is in contact with this catalyst (≈5 Vol%). In the supported monolayer, there are three structurally inequivalent oxygen sites also present on the V_2O_5(001) surface: the single coordinated oxygen O(1), the

Table 1. Predicted and Experimental Bond Distances for Supported Isolated Systems

V_2O_5-iso-TiO_2	V−O(1) (Å)	V−O(2) (Å)	V−O(2)* (Å)
this work	1.61	1.80	1.77
ref 21	1.58	1.78	1.76
W_2O_6-iso-TiO_2	W−O(1) (Å)	W−O(2) (Å)	W−O(2)* (Å)
this work	1.74	1.91−2.01	NA
ref 45	1.72	1.95−1.94	1.91−1.89
VWO_5-iso-TiO_2	V−O(1); W−O(1) (Å)	W−O(2)−V (Å)	W−O(2)*; V−O(2)* (Å)
this work	1.61; 1.72	1.88; 1.85	1.75; 1.81

dx.doi.org/10.1021/jp407794g | J. Phys. Chem. C 2013, 117, 24397−24406

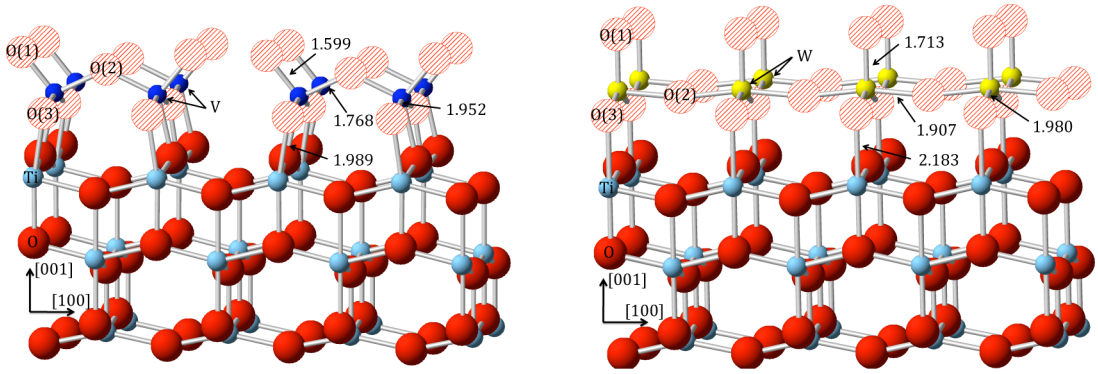

Figure 2. Supported monolayer systems: V_2O_5-mon-TiO_2(001) and WO_3-mon-TiO_2(001) surfaces. Red are oxygen atoms and light blue are Ti atoms from TiO_2, red dashed are oxygen atoms, dark blue are V atoms, and yellow are W atoms from the V_2O_5 and WO_3 supported phases. The three inequivalent atoms are labeled according to their coordination number: O(1), O(2), and O(3) if they are single, double, or triple coordinated, respectively.

bridging O(2) oxygen atom (V−O(2)−V), and the anchoring O(3) oxygen atom that is coordinated with two V atoms and one Ti atom from the support. These atoms are shown in Figure 2, and a comparison of the bond distances of this supported vanadia monolayer phase with a previous DFT study is shown in Table 2.

Table 2. Predicted and Experimental Bond Distances for Supported Monolayer Systems

V_2O_5-mon-TiO_2	V−O(1) (Å)	V−O(2) (Å)	V−O(2)* (Å)
this work	1.61	1.80	1.77
ref 19	1.61	1.77	NA
WO_3-mon-TiO_2	W−O(1) (Å)	W−O(2) (Å)	W−O(2)* (Å)
WO_3(001)	1.71	1.98	1.87
bulk-WO_3	1.73	2.01	1.87

The better match between the bond distances of TiO_2 (1.93−1.98 Å, distorted tetrahedra) and WO_3(001) (1.81−1.98 Å, orthorhombic) compared to the TiO_2 and V_2O_5(001) (1.78−2.02 Å, orthorhombic) could justify our choice of the modeling of the former system as another epitaxially grown film. The orthorhombic phase of WO_3 is stable between 300 and 710 °C, and it is the phase chosen to model the WO_3 since it is within the range of operational temperatures for the SCR unit (e.g., 150−400 °C). The changes in the bond distances of the WO_3 phase in the WO_3−TiO_2(001) surfaces with respect to the bulk WO_3 phase are summarized in Table 2. The bulk WO_3 was chosen as a reference state because to the authors knowlegde this is the first DFT study of WO_3−TiO_2(001) systems, so no other bond distances are available for comparison. These small changes in the bond distances of the supported WO_3 phase validates our initial approximation of modeling this supported phase as an epitaxially grown film.

Since the surface composition has an impact on the reactivity of the SCR catalyst toward Hg oxidation, systems with different ratios of V_2O_5 and WO_3 were modeled. The starting structure was the 100% V_2O_5−TiO_2 system, which contains four units of V_2O_5. By replacing one of the four V_2O_5 units by one WO_3 unit, the 75% V_2O_5−25% WO_3−TiO_2 surface was obtained. This process was repeated until all the V_2O_5 units were replaced by WO_3 units leading to the 100% WO_3−TiO_2 surface. The composition of the different systems expressed in the % of each phase can be converted to units of mmol of each phase per 100 m^2 of the support surface area for an easier comparison against experimental results. These conversions are summarized in Table 3, and four out the five structures modeled are represented in Figure 3.

Table 3. Conversion of the Catalyst Compositions from % to mmol/100 m^2 of TiO_2(001)

composition (%)	composition (mmol/100 m^2 of TiO_2(001))
100% V_2O_5−TiO_2	0.57 mmol of V_2O_5
75% V_2O_5−25% WO_3−TiO_2	0.43 mmol V_2O_5−0.15 mmol WO_3
50% V_2O_5−50% WO_3−TiO_2	0.28 mmol V_2O_5−0.28 mmol WO_3
25% V_2O_5−75% WO_3−TiO_2	0.14 mmol V_2O_5−0.43 mmol WO_3
100% WO_3−TiO_2	0.57 mmol WO_3

Following the procedure as in Vittadini et al.,[21] the relative stability of the supported systems was analyzed based on the formation energies, using the (1 × 4)-reconstructed-TiO_2(001) surface and V_2O_5 bulk phase, $E_{nVO_{2.5}}$, as references. The energy of the former was obtained by adding the reconstruction energy, E_{recon}, to the energy of the (1 × 1)-unreconstructed (4 × 2) TiO_2(001) surface, E_{uncon}. The formation energy, E_{form}, is defined in eq 1:

$$E_{form} = E_{uncon} - [E_{nV_2O_5} + E_{TiO_2} + E_{recon}] \quad (1)$$

The formation energies are −1.27, −0.90, −0.89, −1.17, and −1.25 eV for 100−0%, 75−25%, 50−50%, 25−75%, and 0−100% V_2O_5−WO_3−TiO_2 systems, respectively. From the formation energies, it is clear that both binary systems (100% V_2O_5 and 100% WO_3 supported systems) are more stable than the ternary systems. The structural mismatch between the V_2O_5 and WO_3 monolayer is responsible for the weaker formation energies of the ternary systems but may lead to higher reactivities.

Vibrational analysis was performed to check the validity of the chosen structures as models of the binary and ternary supported monolayer systems. The wavenumbers corresponding to vibrational modes of V−O(1), V−O(2)−V, W−O(1), W−O(2)−W, and V−O(2)−W stretching modes were well-resolved and decoupled from other vibrations. For the pure vanadia systems, the V−O(1) streching frequency calculated is 1091 cm^{-1}, while the V−O(2)−V vibrates longitudinal or transversal leading to 827 and 565 cm^{-1}, respectively. Experimental vibrational frequencies obtained with Raman spectroscopy yield 1012 cm^{-1} for the stretching V−O(1)

dx.doi.org/10.1021/jp407794g | J. Phys. Chem. C 2013, 117, 24397−24406

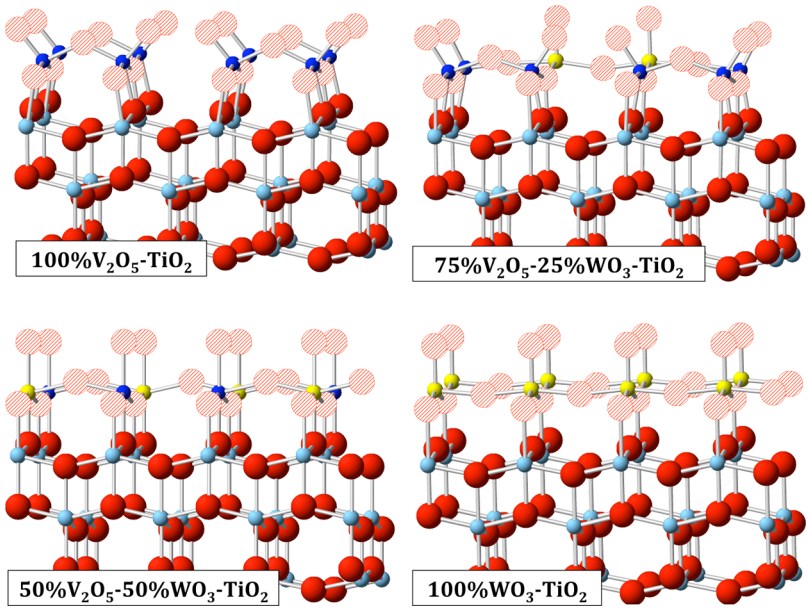

Figure 3. Monolayer V_2O_5–WO_3–TiO_2 structure with different V_2O_5/WO_3 ratios. Dark blue are V atoms, yellow are W atoms, red dashed are O atoms from the supported phase, light blue are Ti atoms, and red are O atoms from the TiO_2 support. Left to right, starting from the top: 100% V_2O_5, 75% V_2O_5–25% WO_3, 50% V_2O_5–50% WO_3, 100% WO_3 supported systems.

mode; there is no vibrational frequency reported for the V–O(2)–V bonds.[11] For the pure tungsten oxide systems, the W–O(1) stretching frequency was calculated as 1016 cm^{-1} while for the W–O(2)–W bond, two frequencies were calculated, i.e., 949 cm^{-1} for the transverse and 809 cm^{-1} longitudinal, respectively. The vibrational frequency reported experimentally using Raman is 1015 cm^{-1} for the W–O(1) strecthing mode for outgassed dry samples.[3] The shift in the vibrational frequencies obtained in our calculations for the vanadia systems could be due to the experimental conditions (humid vs dry). In general, the results from the vibrational analysis showed reasonable agreement with the available experimental data, validating the models chosen to represent high-loading SCR catalysts.

Effect of the Surface Composition and Surface Coverage on the Reactivity toward Hg Oxidation. Both surface composition and degree of coverage of the active phases have an impact on the reactivity of the SCR catalyst since they affect the type and number of active sites responsible for the catalyst activity. Elucidating the effect of these two factors on the reactivity toward Hg oxidation requires analyzing the adsorption energies of Hg, HgCl, HCl, and Cl$^\bullet$ species, which are likely to be involved in the oxidation mechanism. Since HgCl is a radical species, it is not expected to be stable in the gas phase but rather is likely to exist as a surface-bound intermediate, as indicated by previous studies on Hg adsorption across carbon surfaces.[47,48] This intermediate species may also exist to some extent in the gas phase[49−51] at elevated temperatures and may react with surface-adsorbed Cl atoms to form $HgCl_2$ or adsorb on the surface prior to reaction with a gas-phase Cl$^\bullet$ radical to form $HgCl_2$. The adsorption energies have been calculated using eq 2:

$$E_{ad}^{X} = E_{system} - (E_{gas\text{-}phase}^{X} + E_{clean}) \quad (2)$$

where E_{system}, $E_{gas\text{-}phase}^{X}$, and E_{clean} are the calculated energies of the surface after adsorption of X atom/molecule, the energy of X in the gas-phase, and the energy of the clean surface prior to adsorption, respectively.

Effect of the Surface Composition. The effect of surface composition on the reactivity of the catalyst has been examined by comparing the adsorption energies of different gas species on surfaces with varying V_2O_5/WO_3 ratios. This analysis will be limited to the most reactive sites for each surface so the first step is the identification of these sites. The 75% V_2O_5–25% WO_3–TiO_2(001) surface is chosen for this initial anlysis since it contains all the different adsorption sites present in both binary and ternary systems.

Figure 4 shows the three different surface oxygen atoms that lead to five different adsorption sites depending on the nature of the metal atoms they are coordinated (V or/and W atoms depending on the surface composition analyzed). The different adsorption sites are labeled as A for O(1)–W site, B for O(2)–VV site, C for O(2)–VW site, D for O(1)–V site, and E for the

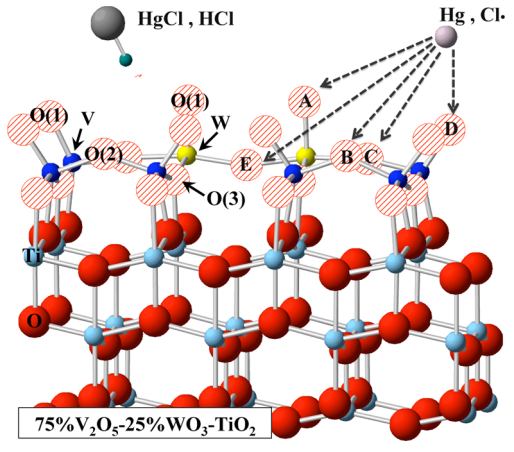

Figure 4. Adsorption configuration tested for single adatom (Hg and Cl$^\bullet$) and admolecule species (HCl and HgCl) on the supported monolayer systems.

dx.doi.org/10.1021/jp407794g | J. Phys. Chem. C 2013, 117, 24397−24406

Table 4. Adsorption Energies (eV) of Hg, HCl, HgCl, and Cl• on A, B, C, D, and E Adsorption Sites for 75% V_2O_5–25% WO_3–TiO_2(001)

Hg–O(1)–V (D)	Hg–O(1)–W (A)	Hg–O(2)–VV (B)	Hg–O(2)–VW (C)	Hg–O(2)–WW (E)
−0.17	−0.19	−0.03	−0.20	−0.15
Cl•–O(1)–V (D)	Cl•–O(1)–W (A)	Cl•–O(2)–VV (B)	Cl•–O(2)–VW (C)	Cl•–O(2)–WW (E)
−1.03	−0.79	−0.26	−0.33	−0.31
HCl–O(1)–V (D)	HCl–O(1)–W (A)	HCl–O(2)–VV (B)	HCl–O(2)–VW (C)	HCl–O(2)–WW (E)
−0.12	−0.20	0.06	−0.05	−0.17
HgCl–O(1)–V (D)	HgCl–O(1)–W (A)	HgCl–O(2)–VV (B)	HgCl–O(2)–VW (C)	HgCl–O(2)–WW (E)
−1.95	−1.69	−1.71	−1.78	−1.85

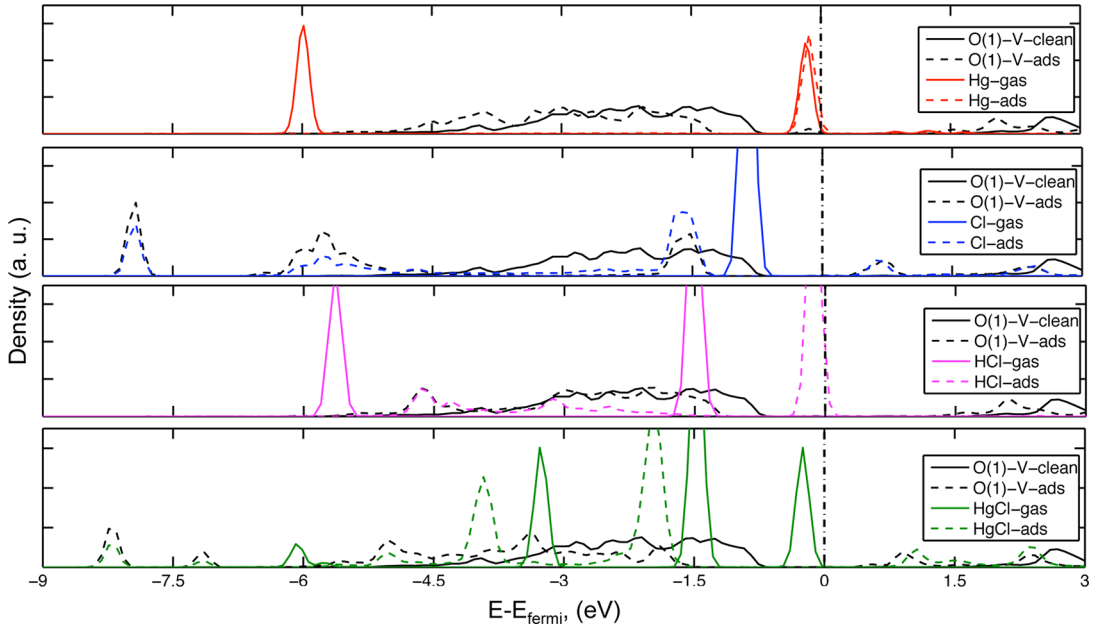

Figure 5. PDOS of s- and p-orbitals for O(1), Hg, Cl•, HCl, and HgCl before and after adsorption in the 75% V_2O_5–25% WO_3. Solid and dashed lines correspond to species and surface O(1) atom before and after adsorption, respectively.

O(2)–WW site. The binding mechanism of Hg, Cl•, HCl, and HgCl on these sites was investigated by representing the adsorbed species as an admolecule placed on top, slightly tilted from the vertical position. The values of the adsorption energies are summarized in Table 4 for the surface composition 75% V_2O_5–25% WO_3–TiO_2(001).

A comparison of the adsorption energies among the four species indicates that HgCl has the highest affinity for the surface, followed by Cl•, HCl, and Hg in decreasing order of bonding strength. The preferred orientation for the HgCl molecule is the configuration in which the chlorine atom is singly coordinated, i.e., Cl–Hg–surface. The Cl• radical interacts vertically as an adatom with the surface oxygen atoms leading to relative strong adsorption energies. The adsorption of HCl on the surface oxygen atoms was investigated in the same configuration as HgCl (i.e., the chlorine atom is singly coordinated as Cl–H–surface) since this configuration was energetically favored. The stability of Hg in the gas phase of coal-fired flue gas explains the lowest adsorption energies of all of the adsorbates investigated. It has been suggested[35,36] that Hg is displaced on the surface by HCl when both gases are injected in the flue gas. Our results agree with these experimental findings, since lower adsorption energies were obtained for Hg compared to HCl.

The results presented in Table 4 indicate a higher reactivity of the O(1) atom (single coordinated); therefore, for simplicity of the analysis only interactions of the four gas species with this oxygen surface atom was further analyzed. The projected density of states (PDOS) analysis was carried out for a deeper understanding on the electronic changes upon adsorption. Figure 5 shows the projected density of the s- and p-orbitals of the O(1) and the Hg, Cl•, HCl, and HgCl before and after adsorption.

The bonding strength between adspecies and surface atoms can be analyzed by comparing the degree of overlapping between the density peaks and their position with respect the Fermi level (located at 0 eV in Figure 5). The analysis of the adsorption energies indicated that HgCl has the highest adsorption energies followed by Cl•, HCl, and Hg. The same trend can be seen in Figure 5, with the highest degree of overlapping between the peaks of the HgCl molecule and O(1) surface atom upon adsorption (black and green dashed lines). These peaks are located at lower energies than those generated from the interaction of Cl• with the surface O(1) atom, which follows in adsorption strength (black and blue dashed lines). The peaks of HCl, Cl•, and HgCl split and broaden upon adsorption due to the strong interaction with the surface oxygen atom. This effect is not seen in the case of Hg adsorption, which also present a negligle overlap of the density peaks, corresponding to weak physisorption.

The effect of the surface composition on the reactivity of the high-loading SCR catalys was studied by the analysis of the

dx.doi.org/10.1021/jp407794g | J. Phys. Chem. C 2013, 117, 24397−24406

adsorption energies of these four gas species with the O(1) atom, and they are summarized in Table 5.

Table 5. Adsorption Energies (eV) of Hg, Cl•, HCl, and HgCl Species on the O(1) Oxygen Atoms for TiO_2-Supported Monolayer Systems

E_{ads}	100% V_2O_5	75% V_2O_5–25% WO_3	50% V_2O_5–50% WO_3	25% V_2O_5–75% WO_3
Hg–O(1)–V	0.12	−0.17	−0.13	−0.17
Cl–O(1)–V	−0.30	−1.03	−1.01	−0.77
HCl–O(1)–V	−0.01	−0.12	−0.12	−0.13
HgCl–O(1)–V	−1.57	−1.95	−1.87	−1.91
E_{ads}	100% WO_3	75% V_2O_5–25% WO_3	50% V_2O_5–50% WO_3	25% V_2O_5–75% WO_3
Hg–O(1)–W	−0.13	−0.19	−0.12	−0.15
Cl–O(1)–W	−0.50	−0.80	−0.78	−1.06
HCl–O(1)–W	−0.11	−0.20	−0.05	−0.12
HgCl–O(1)–W	−1.86	−1.69	−1.73	−1.71

From the adsorption energies shown in Table 5 it is possible to see that between the two binary systems tested, 100% WO_3–TiO_2 system is more reactive toward Hg, Cl•, HCl, and HgCl than the vanadia-supported systems. However, ternary systems (V_2O_5–WO_3–TiO_2) have higher adsorption energies than binary systems (i.e., 100% V_2O_5–TiO_2 or 100% WO_3–TiO_2). These results agree with experimental studies that show a higher NO_x conversion and higher selectivity to N_2 at lower temperatures in the ternary compared to the binary systems, for a given vanadia loading.[3] This increase in the reactivity of the SCR catalyst upon WO_3 addition is due to the increase of the local reactivity of neighboring O(1)–V adsorption sites. This synergy between the V and W oxide surface species is responsible for the higher reactivity of the ternary catalyst. Among the different catalyst compositions tested, the 75% V_2O_5–25% WO_3–TiO_2 leads to slightly higher adsorption energies, and it corresponds to a catalyst composition of 0.43 mmol of V_2O_5 and 0.15 mmol of WO_3 per 100 m^2 of TiO_2.

Effect of the Surface Coverage. The effect of the surface coverage was determied by comparing the adsorption energies of Hg, Cl•, HCl, and HgCl on the systems representing the TiO_2-supported monolayer and submonolayer sytems. For the low-loading SCR catalyst, the surfaces tested are V_2O_5-iso, W_2O_6-iso, and VWO_5-iso-TiO_2, which allows determining the effect of adding W on the reactivity of these catalysts. The reactivity of these low-loading systems is compared to the activity of the 75% V_2O_5–25% WO_3–TiO_2(001) surface, which present the highest reactivity among the high-loading systems. The adsorption energies of Hg, Cl•, HCl, and HgCl on the O(1) atom on these surfaces are obtained using eq 2 and are summarized in Table 6.

Within the ternary systems tested, Table 6 shows higher adsorption energies in the monolayer system (75% V_2O_5–25% WO_3–TiO_2) than the submonolayer system (VWO_5-iso). The stronger adsorption energies on the monolayer system may lead to higher reactivity of these catalysts. These results agree with experimental results that showed higher catalytic activities for NO_x reduction with increasing V_2O_5 loadings in the SCR catalyst. Alemany et al.[3] studied the effect of the vanadia loading on the catalyst performance for the V_2O_5–WO_3–TiO_2 systems. They showed that increasing vanadia loadings from 0 to 3.56 wt % lead to an increase in the turnover frequency from 0.703×10^{-3} to 6.822×10^{-3} mol of NO converted per s and per mol of V (at 590 K). Another study linking the vanadia loading with the catalyst activity was carried out by Amiridis et al., who showed a reduction in the activation energies from 85 to 45 kJ/mol when the vanadia content in the V_2O_5–TiO_2 system decreased from 5.1 to 0.5 wt%.[8]

However, our DFT results suggest that the observed increase in the reactivity with increasing active phase loadings is not due to a larger number of available adsorption sites, but instead to a change in the geometry and coordination of these sites, which lead to stronger adsorption energies. The smaller number of adsorption sites in the low-loading systems sites is not the limiting factor in the reactivity since the concentration of the Hg, Cl•, HCl, and HgCl is ppb and ppm levels, which are insignificant compared with the number of available adsorption sites.

In our previos work,[41] it was shown that Hg had a negligible interaction with the vanadia oxide dimer, while HgCl had the strongest adsorption, followed by HCl. These results were used to suggest a mechanism for the Hg oxidation that involved Langmuir–Hinshelwood step between HCl and HgCl to produce $HgCl_2$ and a Eley–Rideal step between gas-phase Hg and adsorbed HCl to produce HgCl. The latter step can be justified by the weak Hg–surface interaction and to explain the source of HgCl needed in the former step. As shown in Table 6, the interaction of Hg for the ternary submonolayer system (VWO_5-iso) is still the weakest interaction, followed by HCl and HgCl in increasing adsorption strength. These results suggest that the mechanism proposed previously is still valid for the low-loading systems. However, for the high-loading system (75% V_2O_5–25% WO_3–TiO_2), the interaction of Hg and HCl with the surface yield similar adsorption energies (≈−0.19 eV), with HgCl presenting the highest adsorption energy (−1.95 eV).

The addition of W into the dimer structure of the low loading systems leads to an increase in the reacitivity of the O(1)–W adsorption site toward Cl• and HCl but a slightly decrease for Hg and HgCl. However, similar to the monolayer systems, the addition of W increases the reactivity of neigbouring O(1)–V adsorption site compared to the O(1)–V of the binary system (V_2O_5-iso). To understand the effect on

Table 6. Adsorption Energies (eV) of Hg, Cl•, HCl, and HgCl Molecules on O(1) Oxygen Atoms for the TiO_2-Supported Isolated and Monolayer Systems

	V_2O_5-iso	W_2O_6-iso	VWO_5-iso		75% V_2O_5–25% WO_3	
adsorbent	X–O(1)–V	X–O(1)–W	X–O(1)–V	X–O(1)–W	X–O(1)–V	X–O(1)–W
Hg–O(1)	0.92	−0.01	0.00	0.01	−0.17	−0.19
Cl–O(1)	0.15	−0.39	−0.56	−0.54	−1.03	−0.80
HCl–O(1)	0.79	−0.09	−0.13	−0.09	−0.12	−0.20
HgCl–O(1)	0.02	−0.44	−0.65	−0.11	−1.95	−1.69

dx.doi.org/10.1021/jp407794g | J. Phys. Chem. C 2013, 117, 24397–24406

the reactivity of the local oxygen atoms upon adding a W atom in the dimer structure, Bader charge analysis was performed to correlate the atomic charge of the surface atoms of the dimer with their reactivity.

Bader Charge Analysis for the Low Loading Systems. The Bader charge analysis uses the atoms in molecules (AIM) approach, which defines atomic regions (i.e., Bader volumes) within molecules by spatially resolving the minimum electron density of the system.[52] The charge of each atom is calculated by integrating the electronic density within its Bader volume. Because of the different coordination of the atoms in a surface, the same type of atoms may have different charges and thus different chemical reactivity. Therefore, the Bader charge analysis may be used as a way to predict the reactivity of a given atom within the surface. In this work, the Bader charge analysis is used to determine the electronic changes associated with the addition of W in the neighboring metal site in the submonolayer systems. The atomic charges for the different surface atoms of the submonolayer sytems are summarized in Table 7.

Table 7. Atomic Charge Differences Calculated with Respect to the Number of Valence Electrons for Supported Isolated Systems

surface atom	V_2O_5-iso-TiO_2	VWO_5-iso-TiO_2	W_2O_6-iso-TiO_2
V−O(1)	−0.57	−0.58	NA
W−O(1)	NA	−0.70	−0.71
O(2)	−0.88	−0.95	−0.94
O(2)*−V	−0.88	−0.88	NA
O(2)*−W	NA	−0.95	−0.92

The amount of charge transfer from a given metal atom to the surrounding oxygen atoms is based upon the number of valence electrons of the given metall i.e., tungsten and vanadium have 6 and 5 valence electrons, respectively. In the case of the V_2O_5-iso- and W_2O_6-iso-TiO_2 systems, due to symmetry, each oxygen atom surrounding a metal atom (i.e., V or W) has the same charge as the corresponding oxygen atom on the other metal atom of the dimer. This is not the case for the VWO_5-iso-TiO_2 system where the symmetry is removed when tungsten is added. In this case, a higher negative charge exists on the O(1), O(2), and O(2)* oxygen atoms surrounding the W atom since it can donate more electrons. For example, the charge of the O(2) increases from −0.88 in V−O(2)−V dimer to −0.95 for the V−O(2)−W dimer.

The charge of the O(1) atom attached to V slightly increases from −0.57 to −0.58 due to the presence of the neighboring W atom. Although this is a small change, it is possible to see an increase in the reactivity of this atom as it is reflected in the larger adsorption energies of this atom toward Hg, $Cl^{\bullet}$, HCl, and HgCl as shown in Table 6. These oxygen atom (O(1)−V) behave as Lewis bases since they can donate the extra electron density to the adsorbed species.

Projected Density of States (PDOS) as a Function of the Composition and Surface Coverage. For a deeper understanding of the changes in the reactivity associated with surface composition and coverage, density of states (DOS) calculations are carried out for the ternary systems within the monolayer and submonolayer regimes. Because of the higher reactivity of the O(1) surface oxygen atom, the total DOS analysis is reduced to the analysis of the projected density of states (PDOS) of the O(1) atom coordinated with either V or W in the surfaces with different coverages.

As shown in Figure 6, there is a significant difference in the PDOS of the O(1) surface oxygen atom in the monolayer and

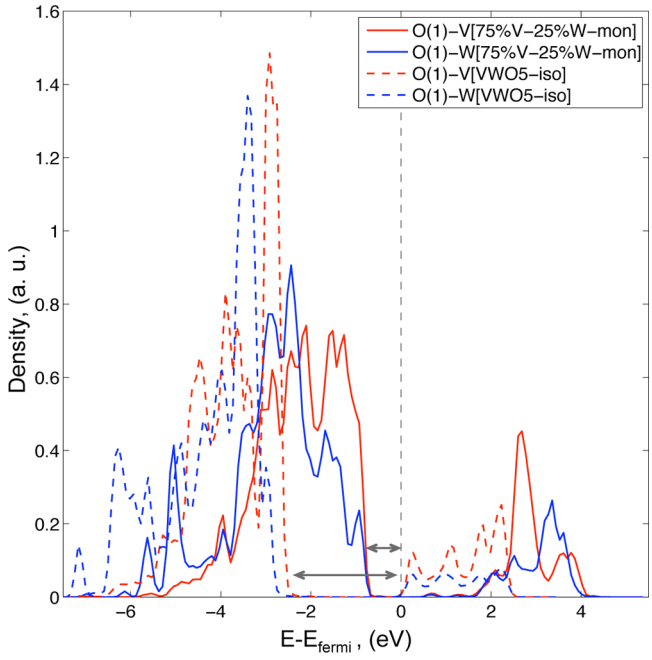

Figure 6. PDOS of p-orbitals for O(1) in the supported monolayer and submonolayer for ternary systems. Blue and red lines correspond to O(1) coordinated to V atom and coordinated to W atom, respectively. Gray arrows indicate difference with respect to the Fermi level.

submonolayer regimes (solid and dashed lines, respectively). Comparing the contribution of the O(1) atom to the valence band, it is possible to see that in the case of monolayer systems the positions of the p-orbital peaks are at higher energies and closer to the Fermi level than those in the isolated dimers. The position with respect the Fermi level is marked with a gray arrow. The location of the valence band closer to the Fermi level is an indication of a higher reactivity, validating the adsorption energy results that indicated stronger adsorptions on O(1) atoms in the monolayer systems than in the low-loading systems. The relative shift of the O(1)−V and O(1)−W peaks within each system (high and low loading) is small as it is the change in the adsorption energies of the gas species on these two atoms.

CONCLUSIONS

With the purpose of examining the effect of the surface composition and surface coverage in the reactivity of a commercial SCR catalyst (V_2O_5−WO_3−TiO_2) toward Hg oxidation, two models were used to represent systems with low- and high-loading of the two active phases: V_2O_5 and WO_3.

The effect of the surface coverage was studied by comparing the reactivity of the low- and high-loading systems. This analysis indicated enhanced reactivity of the SCR catalyst toward HgCl, $Cl^{\bullet}$, HCl, and Hg, with increasing loadings of both V_2O_5 and WO_3 phases. While the adsorption of Hg on the surface oxygen atoms is negiglible in the submonolayer systems, it reaches the same order of magnitude as the HCl interaction in the monolayer systems.

dx.doi.org/10.1021/jp407794g | J. Phys. Chem. C 2013, 117, 24397−24406

Understanding the role of WO_3 in the reactivity of the high loading systems was achieved by replacing V_2O_5 units by WO_3 units on the supported monolayer. The adsorption energies of Hg, $Cl^{\bullet}$, HCl, and HgCl on the binary monolayer systems (i.e., $100\%V_2O_5-TiO_2$ or $100\%WO_3-TiO_2$) were compared against ternary systems ($V_2O_5-WO_3-TiO_2$ with different V_2O_5/WO_3 ratios), indicating a higher reactivity of the latter. This increase in the reactivity of the SCR catalyst upon WO_3 addition is due to the increase of the local reactivity of the O(1)−V adsorption sites surrounding the W atoms. Although small differences in the adsorption energies were found among the different surface coverages tested, the 75% V_2O_5−25% WO_3−TiO_2 system (0.43 mmol of V_2O_5 and 0.15 mmol of WO_3 per 100 m^2 of TiO_2 catalyst) has shown the slightly highest reactivity of the ternary systems.

Although this study suggests 75% V_2O_5−25% WO_3−TiO_2 as the optimal V−W−Ti composition toward Hg oxidation, an important and necessary future step is to validate this composition as sufficiently active for the reduction of NO_X. As mentioned in the Introduction, the main function of the SCR catalyst is the reduction of NO_X to N_2; therefore, any change in the composition of the SCR catalyst to improve Hg oxidation should be done within the limits of a good performance toward NO_X reduction. Furthermore, the undesired SO_2 to SO_3 oxidation reactions is also catalyzed across the SCR catalyst, so future work should examine the effect of the catalyst composition on the interaction of SO_2 and SO_3 and their impact in the Hg oxidation. The addition of other metal oxides on the SCR catalyst to further promote the Hg oxidation will be considered by the authors in the future.

AUTHOR INFORMATION

Corresponding Author

*E-mail: wilcoxj@stanford.edu (J.W.).

Notes

The authors declare no competing financial interest.

REFERENCES

(1) UNEP, Mercury, Time to Act; Technical Report, 2013.

(2) United States Environmnetal Protection Agency, E. Mercury and Air Toxics Standards (MATS) for Power Plants; June 21, 2011.

(3) Alemany, L.; Lietti, L.; Ferlazzo, N.; Forzatti, P.; Busca, G.; Giamello, E.; Bregani, F. Reactivity and Physicochemical Characterization of V_2O_5-WO_3/TiO_2 De-NOx Catalysts. *J. Catal.* **1995**, *155*, 117−130.

(4) Lietti, L.; Forzatti, P.; Bregani, F. Steady-State and Transient Reactivity Study of TiO_2-Supported V_2O_5-WO_3 De-NOx Catalysts: Relevance of the Vanadium-Tungsten Interaction on the Catalytic Activity. *Ind. Eng. Chem. Res.* **1996**, *35*, 3884−3892.

(5) Lietti, L.; Nova, I.; Forzatti, P. Selective Catalytic Reduction (SCR) of NO by NH_3 over TiO_2-Supported V_2O_5−WO_3 and V_2O_5−MoO_3 Catalysts. *Top. Catal.* **2000**, *11*, 111−122.

(6) Presto, A.; Granite, E. Survey of Catalysts for Oxidation of Mercury in Flue Gas. *Environ. Sci. Technol.* **2006**, *40*, 5601−5609.

(7) Svachula, J.; Alemany, L.; Ferlazzo, N.; Forzatti, P.; Tronconi, E.; Bregani, F. Oxidation of Sulfur Dioxide to Sulfur Trioxide over Honeycomb DeNoxing Catalysts. *Ind. Eng. Chem. Res.* **1993**, *32*, 826−834.

(8) Amiridis, M. D.; Solar, J. P. Selective Catalytic Reduction of Nitric Oxide by Ammonia over V_2O_5/TiO_2, $V_2O_5/TiO_2/SiO_2$, and V_2O_5-WO_3/TiO_2 Catalysts: Effect of Vanadia Content on the Activation Energy. *Ind. Eng. Chem. Res.* **1996**, *35*, 978−981.

(9) Saleh, R.; Wachs, I.; Chan, S.; Chersich, C. The Interaction of V_2O_5 with TiO_2 (Anatase): Catalyst Evolution with Calcination Temperature and o-Xylene Oxidation. *J. Catal.* **1986**, *98*, 102−114.

(10) Djerad, S.; Tifouti, L.; Crocoll, M.; Weisweiler, W. Effect of Vanadia and Tungsten Loadings on the Physical and Chemical Characteristics of V_2 O_5-WO_3/TiO_2 Catalysts. *J. Mol. Catal. A: Chem.* **2004**, *208*, 257−265.

(11) Sun, C.; Dong, L.; Yu, W.; Liu, L.; Li, H.; Gao, F.; Dong, L.; Chen, Y. Promotion Effect of Tungsten Oxide on SCR of NO with NH_3 for the V_2O_5-$WO_3/Ti_{0.5}Sn_{0.5}O_2$ Catalyst: Experiments Combined with DFT Calculations. *J. Mol. Catal. A: Chem.* **2011**, *346*, 29.

(12) Chen, J.; Yang, R. Role of WO_3 in Mixed V_2 O_5-WO_3/TiO_2 Catalysts for Selective Catalytic Reduction of Nitric Oxide with Ammonia. *Appl. Catal. A: Gen.* **1992**, *80*, 135−148.

(13) Goclon, J.; Grybos, R.; Witko, M.; Hafner, J. Relative Stability of Low-Index V_2O_5 Surfaces: a Density Functional Investigation. *J. Phys.: Condens. Matter* **2009**, *21*, 095008.

(14) Goclon, J.; Grybos, R.; Witko, M.; Hafner, J. Relative Stability of Low-Index V_2O_5 Surfaces: a Density Functional Investigation. *J. Phys.: Condens. Matter* **2009**, *21*, 095008.

(15) Negreira, A. S.; Aboud, S.; Wilcox, J. Surface Reactivity of V_2O_5(001): Effects of Vacancies, Protonation, Hydroxylation, and Chlorination. *Phys. Rev. B* **2011**, *83*, 045423.

(16) Blum, R.; Niehus, H.; Hucho, C.; Fortrie, R.; Ganduglia-Pirovano, M.; Sauer, J.; Shaikhutdinov, S.; Freund, H. Surface Metal-Insulator Transition on a Vanadium Pentoxide (001) Single Crystal. *Phys. Rev. Lett.* **2007**, *99*, 226103.

(17) Ganduglia-Pirovano, M.; Sauer, J. Stability of Reduced V_2O_5(001) Surfaces. *Phys. Rev. B* **2004**, *70*, 45422.

(18) Chakrabarti, A.; Hermann, K.; Druzinic, R.; Witko, M.; Wagner, F.; Petersen, M. Geometric and Electronic Structure of Vanadium Pentoxide: A Density Functional Bulk and Surface Study. *Phys. Rev. B* **1999**, *59*, 10583.

(19) Alexopoulos, K.; Hejduk, P.; Witko, M.; Reyniers, M.; Marin, G. Theoretical Study of the Effect of (001) TiO_2 Anatase Support on V_2O_5. *J. Phys. Chem. C* **2010**, *114*, 3115−3130.

(20) Vittadini, A.; Casarin, M.; Sambi, M.; Selloni, A. First-Principles Studies of Vanadia-Titania Catalysts: Beyond the Monolayer. *J. Phys. Chem. B* **2005**, *109*, 21766−21771.

(21) Vittadini, A.; Selloni, A. Periodic Density Functional Theory Studies of Vanadia-Titania Catalysts: Structure and Stability of the Oxidized Monolayer. *J. Phys. Chem. B* **2004**, *108*, 7337−7343.

(22) Calatayud, M.; Mguig, B.; Minot, C. A Periodic Model for the V_2O_5-TiO_2 (Anatase) Catalyst. Stability of Dimeric Species. *Surf. Sci.* **2003**, *526*, 297−308.

(23) Calatayud, M.; Minot, C. Reactivity of the Oxygen Sites in the V_2O_5/TiO_2 Anatase Catalyst. *J. Phys. Chem. B* **2004**, *108*, 15679−15685.

(24) Vittadini, A.; Casarin, M.; Selloni, A. First Principles Studies of Vanadia-Titania Monolayer Catalysts: Mechanisms of NO Selective Reduction. *J. Phys. Chem. B* **2005**, *109*, 1652−1655.

(25) Sauer, J.; Döbler, J. Structure and Reactivity of V_2O_5: Bulk Solid, Nanosized Clusters, Species Supported on Silica and Alumina, Cluster Cations and Anions. *Dalton Trans.* **2004**, 3116−3121.

(26) Broclawik, E.; Góra, A.; Najbar, M. The Role of Tungsten in Formation of Active Sites for No SCR on the VWO Catalyst Surface - Quantum Chemical Modeling (DFT). *J. Mol. Catal. A: Chem.* **2001**, *166*, 31−38.

(27) Senior, C. L.; Helble, J. J.; Sarofim, A. F. Emissions of Mercury, Trace Elements, and Fine Particles from Stationary Combustion Sources. *Fuel Process. Technol.* **2000**, *65*, 263−288.

(28) Wachs, I.; Weckhuysen, B. Structure and Reactivity of Surface Vanadium Oxide Species on Oxide Supports. *Appl. Catal., A* **1997**, *157*, 67−90.

(29) Went, G.; Oyama, S.; Bell, A. Laser Raman Spectroscopy of Supported Vanadium Oxide Catalysts. *J. Phys. Chem.* **1990**, *94*, 4240−4246.

(30) Olthof, B.; Khodakov, A.; Bell, A.; Iglesia, E. Effects of Support Composition and Pretreatment Conditions on the Structure of Vanadia Dispersed on SiO_2, Al_2O_3, TiO_2, ZrO_2, and HfO_2. *J. Phys. Chem. B* **2000**, *104*, 1516−1528.

(31) Kozlowski, R.; Pettifer, R.; Thomas, J. X-ray Absorption Fine Structure Investigation of Vanadium(V) Oxide-Titanium(IV) Oxide Catalysts. 2. The Vanadium Oxide Active Phase. *J. Phys. Chem.* **1983**, *87*, 5176−5181.
(32) Haber, J.; Kozlowska, A.; Kozlowski, R. The Structure and Redox Properties of Vanadium Oxide Surface Compounds. *J. Catal.* **1986**, *102*, 52−63.
(33) Niksa, S.; Fujiwara, N. A Predictive Mechanism for Mercury Oxidation on Selective Catalytic Reduction Catalysts under Coal-Derived Flue Gas. *J. Air Waste Manage.* **2005**, *55*, 1866−1875.
(34) Senior, C.; Linjewile, T. Oxidation of Mercury across SCR Catalyst in Coal-Fired Power Plants Burning Low Rank Fuels; Technical Report, 2003.
(35) He, S.; Zhou, J.; Zhu, Y.; Luo, Z.; Ni, M.; Cen, K. Mercury Oxidation over a Vanadia-Based Selective Catalytic Reduction Catalyst. *Energy Fuels* **2008**, *23*, 253−259.
(36) Eom, Y.; Jeon, S.; Ngo, T.; Kim, J.; Lee, T. Heterogeneous Mercury Reaction on a Selective Catalytic Reduction (SCR) Catalyst. *Catal. Lett.* **2008**, *121*, 219−225.
(37) Kresse, G.; Furthmüller, J. Efficiency of ab-Initio Total Energy Calculations for Metals and Semiconductors Using a Plane-Wave Basis Set. *Comput. Mater. Sci.* **1996**, *6*, 15−50.
(38) Perdew, J.; Burke, K.; Ernzerhof, M. Generalized Gradient Approximation Made Simple. *Phys. Rev. Lett.* **1996**, *77*, 3865−3868.
(39) Blochl, P. Projector Augmented-Wave Method. *Phys. Rev. B* **1994**, *50*, 17953−17979.
(40) Monkhorst, H.; Pack, J. Special Points for Brillouin-Zone Integrations. *Phys. Rev. B* **1976**, *13*, 5188−5192.
(41) Suarez Negreira, A.; Wilcox, J. DFT Study of Hg Oxidation across Vanadia-Titania SCR Catalyst under Flue Gas Conditions. *J. Phys. Chem. C* **2013**, *117*, 1761−1772.
(42) Sutton, L. E. *Tables of Interatomic Distances and Configuration in Molecules and Ions: Supplement 1956−59; Chemical Society*, 1965.
(43) Kaupp, M.; von Schnering, H. G. Origin of the Unique Stability of Condensed-phase Hg_{22}^{+}. An ab Initio Investigation of MI and MII Species (M = Zn, Cd, Hg). *Inorg. Chem.* **1994**, *33*, 4179−4185.
(44) Bondarchuk, O.; Huang, X.; Kim, J.; Kay, B. D.; Wang, L.-S.; White, J.; Dohnálek, Z. Formation of Monodisperse $(WO_3)_3$ Clusters on TiO_2 (110). *Angew. Chem., Int. Ed.* **2006**, *45*, 4786−4789.
(45) Huang, X.; Zhai, H.-J.; Waters, T.; Li, J.; Wang, L.-S. Experimental and Theoretical Characterization of Superoxide Complexes $[W_2O_6\ (O_2^-)]$ and $[W_3O_9\ (O_2^-)]$: Models for the Interaction of O_2 with Reduced W Sites on Tungsten Oxide Surfaces. *Angew. Chem., Int. Ed.* **2006**, *45*, 657−660.
(46) Zhai, H.-J.; Huang, X.; Cui, L.-F.; Li, X.; Li, J.; Wang, L.-S. Electronic and Structural Evolution and Chemical Bonding in Ditungsten Oxide Clusters: $W_2O_n^-$ and W_2O_n (n = 1−6). *J. Phys. Chem. A* **2005**, *109*, 6019−6030.
(47) Padak, B.; Brunetti, M.; Lewis, A.; Wilcox, J. Mercury Binding on Activated Carbon. *Environ. Prog.* **2006**, *25*, 319−326.
(48) Padak, B.; Wilcox, J. Understanding Mercury Binding on Activated Carbon. *Carbon* **2009**, *47*, 2855−2864.
(49) Sliger, R.; Kramlich, J.; Marinov, N. Towards the Development of a Chemical Kinetic Model for the Homogeneous Oxidation of Mercury by Chlorine Species. *Fuel Process. Technol.* **2000**, *65*, 423−438.
(50) Horne, D.; Gosavi, R.; Strausz, O. Reactions of Metal Atoms. I. The Combination of Mercury and Chlorine Atoms and the Dimerization of HgCl. *J. Chem. Phys.* **1968**, *48*, 4758.
(51) Wilcox, J. A. Kinetic Investigation of High-Temperature Mercury Oxidation by Chlorine. *J. Phys. Chem. A* **2009**, *113*, 6633−6639.
(52) Sanville, E.; Kenny, S.; Smith, R.; Henkelman, G. Improved Grid-Based Algorithm for Bader Charge Allocation. *J. Comput. Chem.* **2007**, *28*, 899−908.